MICROCOPY RESOLUTION TEST CHART
NATIONAL BUREAU OF STANDARDS-1963-A

(12)

AD A138912

Thermal and Nonthermal Phenomena in Solar Flare Loops at 20 cm Wavelength and in X Rays

E. J. SCHMAHL and M. R. KUNDU
Astronomy Program
University of Maryland
College Park, Maryland 20742

and

P. B. LANDECKER and D. L. McKENZIE
Space Sciences Laboratory
Laboratory Operations
The Aerospace Corporation
El Segundo, California 90245
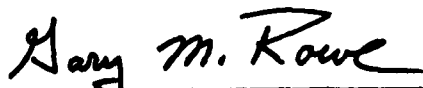
15 December 1983

DTIC
S

DTIC FILE COPY

Prepared for

SPACE DIVISION
AIR FORCE SYSTEMS COMMAND
Los Angeles Air Force Station
P.O. Box 92960, Worldway Postal Center
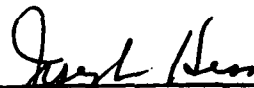Los Angeles, California 90009

84 03 18 028

This report was submitted by The Aerospace Corporation, El Segundo, CA 90245, under Contract No. F04701-83-C-0084 with the Space Division, P.O. Box 92960, Worldway Postal Center, Los Angeles, CA 90009. It was reviewed and approved for The Aerospace Corporation by H. R. Rugge, Director, Space Sciences Laboratory. Captain Gary M. Rowe, SD/YCM, was the project officer for the Mission-Oriented Investigation and Experimentation (MOIE) program.

This report has been reviewed by the Public Affairs Office (PAS) and is releasable to the National Technical Information Service (NTIS). At NTIS, it will be available to the general public, including foreign nationals.

This technical report has been reviewed and is approved for publication. Publication of this report does not constitute Air Force approval of the report's findings or conclusions. It is published only for the exchange and stimulation of ideas.

Gary M. Rowe, Captain, USAF
Project Officer

Joseph Hess, GM-15, Director
West Coast Office, Air Force
Space Technology Center

REPORT DOCUMENTATION PAGE	READ INSTRUCTIONS BEFORE COMPLETING FORM

1. REPORT NUMBER	2. GOVT ACCESSION NO.	3. RECIPIENT'S CATALOG NUMBER
SD-TR-83-95	A128912	

4. TITLE *(and Subtitle)*	5. TYPE OF REPORT & PERIOD COVERED
THERMAL AND NONTHERMAL PHENOMENA IN SOLAR FLARE LOOPS AT 20 cm WAVELENGTH AND IN X RAYS	
	6. PERFORMING ORG. REPORT NUMBER
	TR-0084(4940-01)-2

7. AUTHOR(*s*)	8. CONTRACT OR GRANT NUMBER(*s*)
E. J. Schmahl, M. R. Kundu, P. B. Landecker, and D. L. McKenzie	F04701-83-C-0084

9. PERFORMING ORGANIZATION NAME AND ADDRESS	10. PROGRAM ELEMENT, PROJECT, TASK AREA & WORK UNIT NUMBERS
The Aerospace Corporation El Segundo, California 90245	

11. CONTROLLING OFFICE NAME AND ADDRESS	12. REPORT DATE
Space Division Los Angeles Air Force Station Los Angeles, California 90009	15 December 1983
	13. NUMBER OF PAGES
	23

14. MONITORING AGENCY NAME & ADDRESS*(if different from Controlling Office)*	15. SECURITY CLASS. *(of this report)*
	Unclassified
	15a. DECLASSIFICATION/DOWNGRADING SCHEDULE

16. DISTRIBUTION STATEMENT *(of this Report)*

Approved for public release; distribution unlimited.

17. DISTRIBUTION STATEMENT *(of the abstract entered in Block 20, if different from Report)*

18. SUPPLEMENTARY NOTES

19. KEY WORDS *(Continue on reverse side if necessary and identify by block number)*

Solar flare loops
Solar radio emission
Solar X rays

20. ABSTRACT *(Continue on reverse side if necessary and identify by block number)*

We present X-ray images from the P78-1 satellite for a long-lasting burst at 20-cm wavelength mapped with the Very Large Array on 19 May 1979 by Velusamy and Kundu (1981). The decimeter wave observations were originally interpreted in terms of two models, one invoking thermal electrons radiating at low harmonics of the gyrofrequency, and the other invoking mildly relativistic electrons emitting gyrosynchrotron radiation. If →cont

DD FORM 1473
(FACSIMILE)

19. KEY WORDS (Continued)

20. ABSTRACT (Continued)

indeed the 20 cm source is thermal, it should also be visible in soft X rays, while if it is nonthermal, the soft X-ray emission should be weak or spatially or temporally distinct from the 20 cm burst. We find that only one of the three 20 cm sources was approximately co-spatial with the soft X-ray source, and that it was only partially thermal. The 20 cm burst is therefore primarily decimeter type IV emission from mildly relativistic electrons of the post-flare phase. The long lifetime ($\gtrsim 2^h$) and smooth temporal variation of the burst belie its nonthermal nature and suggest continuous acceleration as well as long term storage of energetic electrons.

PREFACE

1

CONTENTS

1. INTRODUCTION

The solar decimeter wavelength continuum bursts are broadband, extending over hundreds of megahertz and lasting for tens of minutes. They are usually associated with type IV bursts at meter and centimeter wavelengths, although sometimes the weak decimeter wavelength (dcm-λ) continuum events may be associated with centimeter "gradual rise and fall" (GRF) bursts. The decimeter bursts consist of a smooth background continuum emission with the superposition of a succession of bursts of fine temporal structure (Kundu, 1965). The decimeter type IV bursts are usually considered to be extensions of cm-λ type IV bursts (Kundu, 1965). However, the dcm-λ continuum lasts for a much longer time, often until after an associated Hα event is over; this implies that the dcm continuum can sometimes be identified with the post-flare phase.

In the past, impulsive dcm-λ bursts of relatively short duration have been mapped with high spatial resolution in one dimension using the Westerbork Synthesis Radio Telescope (WSRT) by Bregman and Felli (1976) and Drago and Palagi (1980). Velusamy and Kundu (1981) produced the first two-dimensional snapshot synthesized maps on 19 May 1979 of a long lasting (> 2 hours) burst at 20 cm-λ, using the Very Large Array (VLA). They showed evidence that the burst emission originated in post-flare loops mapped at 20 cm and provided estimates of magnetic field strengths within the flaring loop in which the radio emitting electrons were trapped. This event was simultaneously observed in soft X rays by the SOLEX X-ray spectrometer/spectroheliograph aboard the P78-1 satellite. In this report we present a comparison of the burst source observed at 20 cm with the VLA and in soft X rays.

7

The only other reported radio event observed in association with the 20 cm burst was a GRF burst at 3 cm (Solar Geophysical Data, 1979b). Since GRF bursts usually have spectral maxima at wavelengths $\lesssim$ 10 cm (Guidice and Castelli, 1975), the GRF burst probably did not contribute significantly to the emission at 20 cm. Furthermore, the associated X-ray emission was more impulsive than typical GRF X rays (Sheeley et al., 1975), and, as we shall show, the X-ray emission was closely associated with the 20 cm burst.

We would like to point out that the time resolution of the VLA is 10 sec and therefore any fast time structure which might be superimposed on the continuum would be washed out; our study will thus be concerned only with the continuum. The generating mechanism for a type IV continuum emission at 20 cm is primarily gyrosynchrotron radiation from nonthermal ($\gtrsim 10^2$ keV) electrons which are invisible in soft X rays. However, since we are dealing with the burst emission long after the Hα flare is over, it is possible that the burst emission in this post-flare decay phase could be, at least partially, thermal gyroradiation at the first two or three harmonics of the gyrofrequency (Velusamy and Kundu, 1981, henceforth VK). The comparison of the 20 cm and X-ray images of the burst source therefore makes it possible to determine the fraction of thermal and nonthermal emission in the burst.

2. OBSERVATIONS

The period of time during which both VLA observations (VK) and P78-1 X-ray observations overlapped was from 19:55 to 21:50 UT on 19 May 1979. This interval includes two X-ray flares: one of importance M1 (20:35-20:53) and another of importance C7 (21:07-21:25) seen in the GOES 0.5-4 Å and 1-8 Å channels (Solar Geophysical Data, 1979a) and two very faint Hα subflares (S. F. Martin, personal communication) seen at 20:35 very close to the limb in McMath region 15999 (N17 W80) and at 20:41 in McMath 16014 (N17 W50). The two active regions were each bipolar in the same sense (Solar Geophysical Data, 1979b), and most of the 20 cm and X-ray bursts occurred just west of the midpoint between the two regions. A quiescent filament which defines the magnetic geometry between these regions lay north of the midpoint. It showed no changes during the GRF, as confirmed by San Fernando Observatory (S. F. Martin) and Culgoora Observatory (K. Sheridan) filtergrams.

The limbward region, McMath 15999, was at least one rotation old and growing in area from the time of passage across central meridian to the day of observation. The easterly region, McMath 16014, was new, and rapidly growing in size from 11 to 21 May. Regions further west at this latitude crossed the limb before ~ 16 May and were declining in activity (Solar Geophysical Data, 1979b), so they were almost certainly not responsible for the observed activity above the limb.

2.1 THE P78-1 X-RAY EXPERIMENTS

The Solar X-Ray Spectrometer/Spectroheliograph aboard P78-1 has been described by Landecker et al. (1979), Landecker, McKenzie and Rugge (1979),

9

and Landecker and McKenzie (1980). The two (of four) experiments that pro-
vided data for this report were the SOLEX Bragg crystal X-ray spectrometer/
spectroheliograph and the MONEX uncollimated X-ray monitor.

The SOLEX experiment provides either monochromatic raster maps or spectra
in the 3–25 Å range. The raster data presented here include large (45 arc min
square) and small (5 arc min square) rasters made with collimations of 20 arc
sec in X-ray emission lines of Mg XI and Si XIII (SOLEX A) and 60 arc sec in
emission lines of O VII, O VIII and Fe XVII (SOLEX B). The ras· · maps are in
the lines of O VII 21.60 Å, O VIII 18.97 Å, Mg XI 9.17 Å, Fe   :I 15.01 Å and
Si XIII 6.64 Å. The formation temperatures of these lines   ge from ~ 2 x
10^6 to ~ 10^7 K, characteristic of the temperature range fr   · quiescent
corona to the hotter "post-flare loops."

The MONEX experiment consists of a low energy monitor (LEM) for the 1–18
keV range, and a high energy monitor (HEM) for the 18–230 keV range. Each
monitor records 6 channels of pulse height data every 1.024 sec. Figure 1
shows the LEM data along with the GOES data (courtesy of NOAA) for the time
period 19:20–23:10 UT, 19 May 1979. LEM channel 3 (nominally 3.5–5.7 Å; the
LEM has no inflight calibration) is similar to the 1–8 Å range of GOES, and
channel 4 (2.1–3.5 Å) is similar to the 0.5–4 Å range. (The high background
counting rates due to charged particles in the radiation belts have been
suppressed in the MONEX data shown in the figure.)

The impulsive phase of the M1 flare starting at 20:36 was missed by P78-1
during orbital night, but the C7 flare at 21:07 was observed in LEM channels
1–5 and HEM channels 1–3. These events are discussed below along with the
images provided by SOLEX and the VLA.
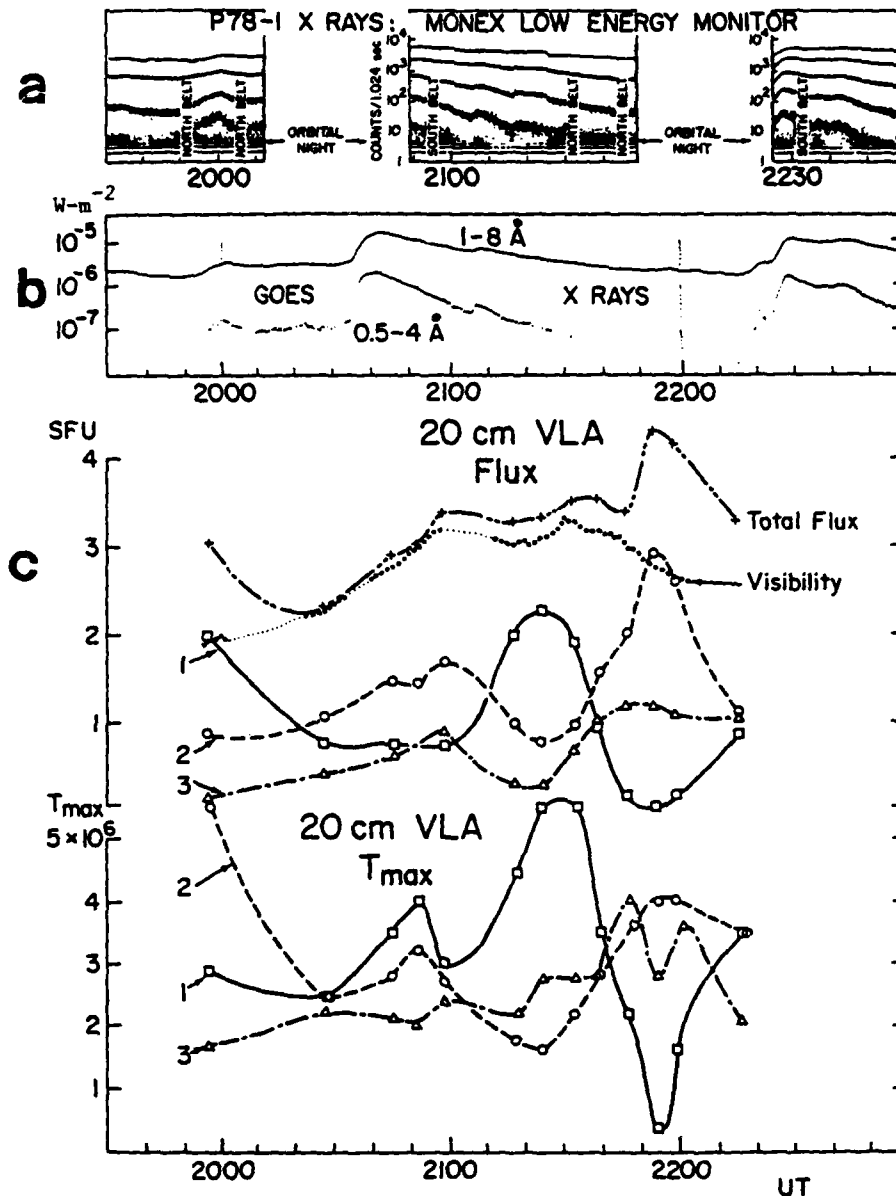
Fig. 1. Low energy monitor (LEM) and GOES data for 19:20 to 23:10 UT on 19 May 1979: (a) MONEX LEM channel data for three orbits of P78-1. Six channels cover 1-18 keV X-ray range; as their energy decreases, counting rates increase. (b) GOES X-ray data, 1-8 Å and 0.5-4 Å (courtesy of NOAA). "Pre-heating" starts at ~20:00, M1 flare at 20:36, and C7 flare at 21:07. (c) Source fluxes (upper graph) and peak brightness temperatures T_m (lower graph) at 20 cm for sources #1, #2, and #3, computed from data of Velusamy and Kundu (1981). Dotted curve shows visibility data for closest baseline pair, which provides the lowest spatial frequency component of the burst.

11

2.2 THE VLA IMAGES

Thirteen maps at 20 cm wavelength were produced by VK for the period 19:55-22:15 UT. Each of these maps incorporates 6 minutes of data, with a beam 12 x 24 arc sec in size. VK identified 3 main sources: #1 on the disk near the southern end of the filament (Figures 2a, b), #2 mostly above the limb and close to region 15999, and #3 to the east of the filament and further inside the limb. These sources are quite variable (see Fig. 4 of VK) and, in particular, source #2 extends to heights much greater than shown in the long integration map of Fig. 2. Using the original tabulations of the radio maps, we have computed time profiles of flux and peak brightness temperature for each source (see Fig. 1). (The curves connecting the points are mainly to guide the eye, and are not meant to indicate interpolations.) The total flux, computed from the entire maps, is very nearly equal to the sum of the 3 source fluxes. That is, other sources and negative noise produced by the map "cleaning" program do not significantly contribute. Furthermore, comparison of the total map flux with the visibility (dotted curve) shows a very close correspondence from 20:27 to 21:45, with the total map flux. (The visibility is the magnitude of the correlation obtained from the closest antenna pair, and therefore shows the lowest spatial frequency component.) Total power records could not be obtained with the VLA in 1979. Differences between the curves before and after the above interval indicate that the single antenna pair used for the visibility data did not map all the flux.

Table I shows the timing of the peaks in X rays and microwaves shown in Fig. 1. There are five main points to note concerning the development of the sources.

12
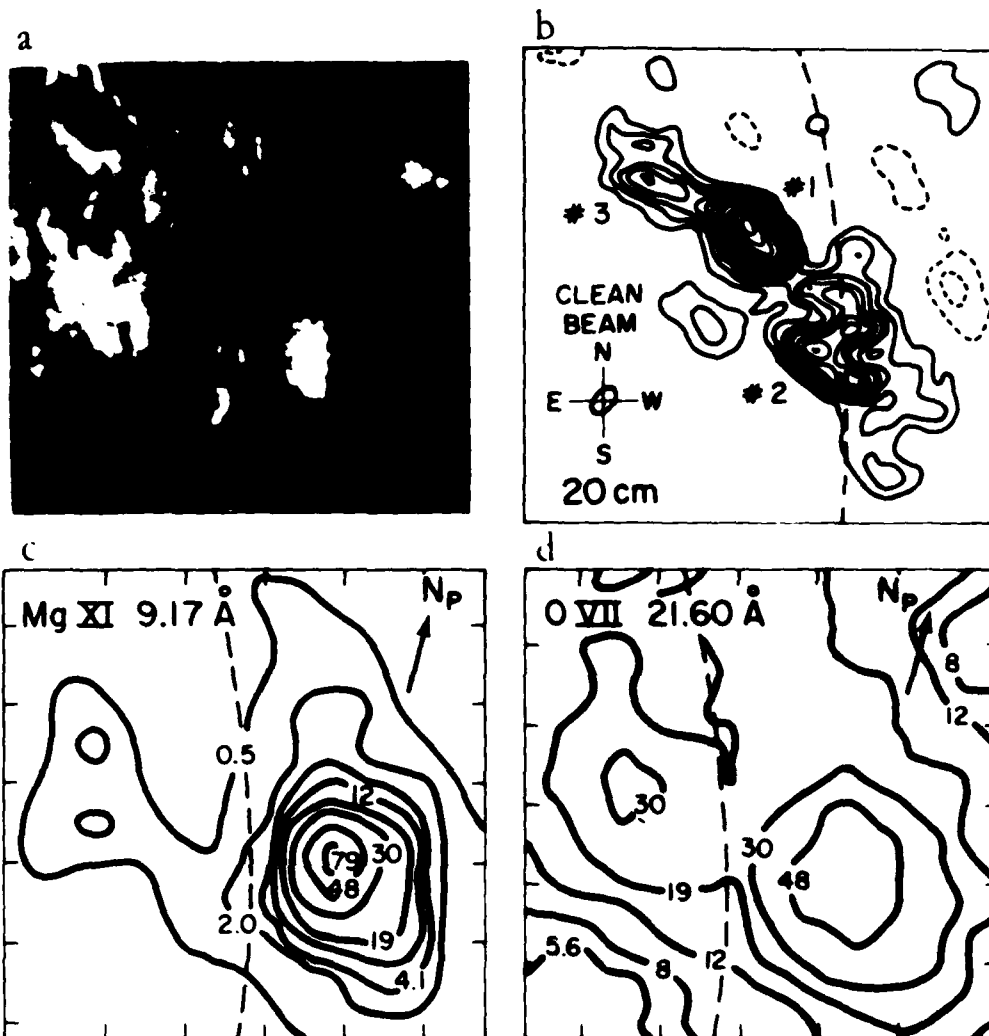
Fig. 2. (a) Hα filtergram at 17:43 (courtesy of Sac Peak National
Observatory): field of view, 6' × 6', co-aligned with 20 cm
map; celestial north is up. (b) Very Large Array 20 cm map for
period 20:17 to 21:56, showing relation of burst sources to Hα.
Figure 4 of Velusamy and Kundu (1981) shows variations in time-
averaged sources. Dashed curve indicates limb and is co-aligned
with dashed curves in (c) and (d); celestial north is up.
(c) Portions of full disk X-ray spectroheliogram in Mg XI at 21:04
during decline of M1 flare. Tick marks on edges of field are at 1'
intervals (collimator full-width at half-maximum field-of-view
is 20"). N$_P$ at arrow indicates solar north. (d) O VII spectro-
heliogram at 21:14. Co-registrations with Mg XI spectrohelio-
gram are indicated by matching tick marks, co-aligned to ~12".
N$_P$ at arrow indicates solar north. Data were recorded through
SOLEX B 60" FWHM collimator.

Table I. Development in X Rays and Microwaves

U.T.	X-Rays	Microwaves
19:55	Onset of X-ray buildup	Rise in 20 cm flux, sources #2, #3
20:36	Peak ratio of hard/soft GOES channels impulsive phase of M1 flare (occurred during P78-1 night)	20 cm source #2 contains most of the flux
20:56	Mg XI raster shows flare at limb	Source #2 has declined
21:07	C7 flare impulsive phase, seen in LEM (1-5) and HRM (1-3) channels	Source #1 rising
21:30	Small rasters show roughly constant emission measure and temperature	Source #1 peaks, while #2 has declined
21:52	Only declining MONEX fluxes	Source #2 peaks.

(a) Before the M1 flare onset at 20:36 there was a general rise in the 20 cm flux, as shown by the visibility curve (and as noted by VK). This appears to be associated with the "pre-heating" in X-rays seen in the P78-1 LEM and GOES channels, starting at ~ 19:55. This pre-flare buildup time profile is very similar to that of the 9.6-19.2 keV OGO-5 profile preceding three flares reported by Kane and Pick (1976), except that the buildup here lasted ~ 30 minutes, as compared with ~ 10 minutes in the earlier flares.

(b) At the onset of the M1 flare, the 20 cm source #2 (on the average, at the limb in Fig. 2 and frequently higher in VK Fig. 4) emitted most strongly. Note that this is in contrast to the pre-flare emission, which was mainly in source 1 (near the filament). This is reminiscent of Kahler's (1979) result that the pre-flare X-ray kernel was not the kernel that flared.

(c) The C7 X-ray flare at 21:07 was associated with a rise in source #1, although the exact rise time is not known to better than ~ 5 minutes.

(d) The decline of the C7 and M1 flares corresponds to a decline in source #1 and a rise in source #2. The peak in total flux at ~ 21:52 was concentrated mainly in the off limb source #2, but was not associated with any soft X-ray enhancement.

(e) During the rises and declines of source #2 described above, there were corresponding rises and declines, with the same phase, in source #3 about 200,000 km further onto the disk. This suggests that there were large scale mar   connections between these two sources.

3. THERMAL PLASMA IN X RAYS AND MICROWAVES

At 20:49 UT, shortly after the onset of the M1 flare, P78-1 came into sunlight. The plasma was rapidly cooling, as judged from the GOES data (Fig. 1b). The ratio of the hard-to-soft X-ray channels (computed from the data provided by N.O.A.A., Fig. 1b) reached a maximum (0.164) at 20:36, and declined by a factor of 0.29 by 20:49. This corresponds roughly to a decrease from 1.5×10^7 K to 1.3×10^7 K, according to spectral estimates derived by Landini and Monsignori Fossi (1979). Full-sun spectroheliograms were obtained by SOLEX, starting at 20:56. Figures 2c and 2d show contours of a 6' x 6' area of the first image at 21:04 in Mg XI 9.17 Å and the second in O VII 21.60 Å at 21:14. (These are the times the spatial maximum was scanned, not start of raster.) The X-ray source appears about 1' above the limb, corresponding to McMath region 15999. However at this time, the brightest 20 cm source was #1, ($T_b \sim 2 \times 10^6$ K) about 2 arc minutes to the northeast. The limb source #2, closely associated spatially with the brightest pixel in Mg XI or O VII, was fainter ($T_b \sim 1 \times 10^6$ K). (It is worthwhile noting that the snapshot map at 21:17 in VK's Fig. 4 shows a better correspondence between the X-ray position and that of source #2 than the time-averaged map of Fig. 2.)

To check the correspondence between brightness temperatures and electron temperatures, we have computed emission measures and electron temperatures from the SOLEX spectroheliograms. These are shown in Table II. SOLEX is equipped with multigrid collimators (McGrath, 1968; Landecker et al., 1979), so the instrument response depends on the position of the source within the field of view and on the source morphology. For SOLEX B, the tabulated fluxes include a factor of 2.9, which converts the maximum measured flux to the flux for the entire emitting region. For SOLEX A the source was compact, with its

17

N-S extent decreasing late in the observing period (see Figure 3). Therefore, we used a correction factor of 5.5 before 20:36 UT, the time of the M1 flare onset, and 2.4 thereafter. The latter factor is quite uncertain since the inferred source size is comparable to the collimator FWHM field of view. There are two additional sources of uncertainty in the data in Table II. Because the line spacing and readout interval for large rasters are coarser than for small, the region included in the brightest large raster pixel may not correspond exactly to that for the brightest small raster pixel. Also, although the SOLEX B response is well understood (McKenzie and Landecker, 1981), the SOLEX A crystal reflectivity is poorly known, especially in the region around the Mg XI lines. Thus the Mg XI fluxes may be underestimated by as much as a factor of two. However, the flux ratios involving Mg XI are far from unity, and the derived temperatures are not very sensitive to the flux values. None of the sources of error discussed here will affect the general conclusions drawn below.

The table includes data from pre-flare small rasters, large rasters during the decline of the M1 flare, and small rasters later on. Whenever two rasters were closely spaced in time, we have computed a temperature based on the line flux ratio in the region surrounding the brightest pixel. The fact that different line pairs give different temperatures may indicate that the plasma was not isothermal. The temperatures thus determined average $\sim 3 \times 10^6$ K. The emission measures, calculated at this temperature and tabulated in the table, vary both as a function of time and as a function of the ion involved. The variation with ion species is another sign that the plasma was not isothermal. As a better indicator of the temperature structure, we have calculated the differential emission measure, $d(EM)/dT$, at the temperature (T_m) of maximum emissivity for each ion. To obtain $d(EM)/dT$, we converted the
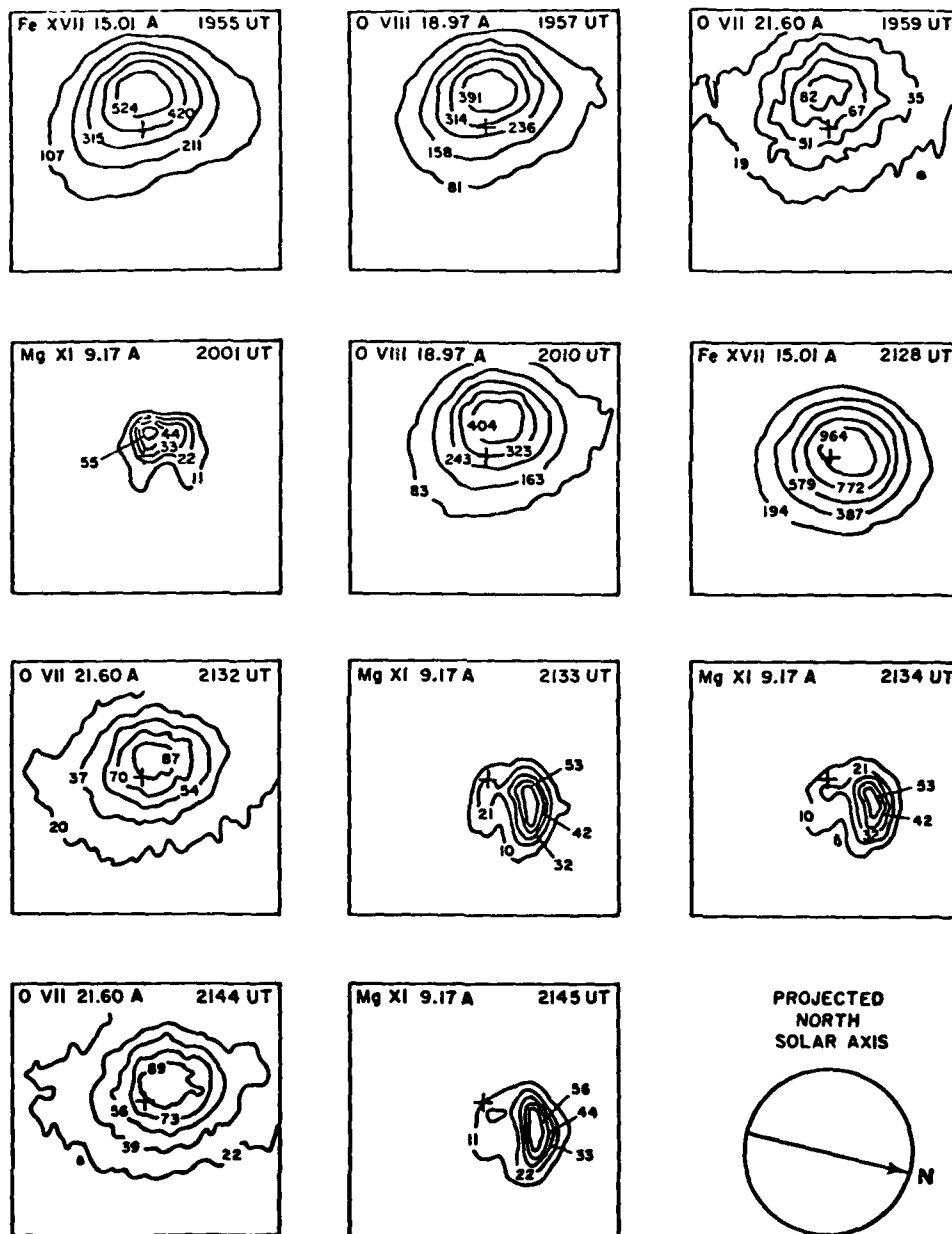
18

Fig. 3. SOLEX small raster spectroheliograms in several X-ray lines during flare-buildup and flare-decline periods. Count rates (per 32 msec) are indicated on contours; crosses denote nominal raster centers. Mg XI SOLEX A rasters are centered 14" S and 28" E of other rasters; pointing was shifted 20" S at 21:25.

Table II. Parameters Derived from SOLEX Raster Maps

H M S (UT)	SOLEX A/B	Ion λ(Å)	BG (cts/32 ms)	P-BG	F (cm⁻² s⁻¹)	N/N+1	T (K)	EM(3.0) (10⁴⁸ cm⁻³)	T_m (10⁶ K)	ΔT (10⁶ K)	$\left(\frac{d}{dT}(EM)\right)^* \tau_m$ (10⁴² cm⁻³ K⁻¹)
19:55:40	B	Fe XVII 15.01	10	609	1.3(6)	0.33	3.6(6)	6.2	4.2	3.5	1.1
19:57:43	B	O VIII 18.97	9	451	3.8(6)	1.5	2.6(6)	4.4	3.0	3.4	1.3
19:58:44	B	O VII 21.60	6	89	2.6(6)			7.1	1.9	1.5	2.4
19:59:46	B	O VII 21.60	8	82	2.4(6)	50.	3.1(6)	6.5	1.9	1.5	2.3
20:00:47	A	Mg XI 9.17	1	81	6.0(4)			10.3	6.0	4.9	0.4
20:01:49	A	Mg XI 9.17	1	66	4.9(4)			8.4	6.0	4.9	0.3
20:10:00	B	O VIII 18.97	9	475	4.0(6)			4.7	3.0	3.4	1.4
21:03:51	A	Mg XI 9.17	0	42	1.4(4)			2.3	6.0	4.9	0.1
21:14:16	B	O VII 21.60	1	76	2.2(6)			6.0	1.9	1.5	2.1
21:26:08	A	Si XIII 6.64	0	5	4.3(2)	1.8(-4)	<2.0(6)	0.6	9.0	8.2	0.002
21:27:10	B	[S XVII] 5.6	13	1155	2.4(6)			11.7	4.2	3.5	2.0

20

Table II. Parameters Derived from SOLEX Raster Maps (Cont.)

H M S (UT)	SOLEX A/B	Ion λ(Å)	BG	P –BG	F	N/N+1	T	EM(3.0)	T_m	ΔT	$\left(\dfrac{d\,(EM)}{dT}\right)^{*}_{T_m}$
			(cts/32 ms)		$(cm^{-2} s^{-1})$		(K)	$(10^{48}\,cm^{-3})$	$(10^{6}\,K)$	$(10^{6}\,K)$	$(10^{42}\,cm^{-3}\,K^{-1})$
21:28:11	B	Fe XVII 15.01	13	1129	2.3(6)	0.40	3.7(6)	11.5	4.2	3.5	2.0
21:29:13	B	O VIII 18.97	9	688	5.7(6)	2.2	2.9(6)	6.8	3.0	3.4	2.0
21:32:17	B	O VII 21.60	6	92	2.6(6)	1.5(2)	2.8(6)	7.3	1.9	1.5	2.5
21:33:18	A	Mg XI 9.17	1	63	2.1(4)			3.5	6.0	4.9	0.1
21:34:20	A	Mg XI 9.17	1	64	2.1(4)	6.8(-3)	2.8(6)	3.5	6.0	4.9	0.1
21:44:35	B	O VII 21.60	1	106	3.0(6)			8.4	1.9	1.5	2.9
21:45:36	A	Mg XI 9.17	1	67	2.2(4)			3.7	6.0	4.9	0.1

*Abundances: Fe, 3.5(-5); O, 7(-4); Mg, 3(-5); Si, 3.5(-5); H, 1.0(0)

flux to emission measure at T_m and divided it by ΔT, the full width at half-maximum of the emissivity-vs-temperature curve. The differential emission measure is shown in the last column of Table II. While the excitation and emission processes for the lines studied here are well understood, the differential emission measure function is subject to errors arising primarily from uncertainties in element abundances (McKenzie and Landecker, 1982). Nevertheless the function can be described qualitatively and compared at different times. In particular, at least above $\sim 3 \times 10^6$ K, it fell with increasing temperature and was very small for $T > 5 \times 10^6$ K at all times.

We can now examine the VLA brightness temperatures with the aid of the information provided by the X-ray maps. For a thermal source of area A the optical depth at 20 cm is

$$\tau \approx 8.9 \times 10^{-20} \frac{EM(T)}{AT^{3/2}}$$

If $\tau > 1$, $T_b = T$ and if $\tau \ll 1$, $T_b = T\tau$. The SOLEX B rasters in Table II are characterized by $T \approx 3 \times 10^6$ K, $EM \approx 4\text{-}12 \times 10^{48}$ cm^{-3}, and $A \approx 2 \times 10^{19}$ cm^2 (diameter $\approx 70''$). This gives $\tau \approx 3\text{-}10$ at 20 cm, so the regions were optically thick. The Mg XI emission came from much smaller regions having higher temperatures. These regions were probably also optically thick at 20 cm. We have computed the blackbody flux at 20 cm expected from source #2 by using the parameters derived from the SOLEX B rasters: $T = 3 \times 10^6$ K and $A = 2 \times 10^{19}$ cm^2. The calculated flux is 1.9 sfu (1 sfu $= 10^{-22}$ W m^{-2} Hz^{-1}), a value comparable to what is shown for source #2 in Figure 1. However, the flux dropped below 1.9 sfu at times (Figure 1), while the X-ray maps changed very little (Figure 3). Further, as we will argue below, at least some of the time the 20 cm emission from source #2 was nonthermal. Thus the thermal emission

should have been below 2 sfu. This can be explained provided that the emissions arose from small (i.e., unresolved) structures that were optically thick at 20 cm. That is, the "filling factor" (source area ÷ beam area) was less than one. An alternative explanation is that, since the emission measure decreased with increasing temperature, the radio telescope may have seen primarily cooler material and hence lower flux. There is some indication that the X-ray loops were higher than the time-average source #2 (see Fig. 2) and therefore that the lower loops seen by the VLA were cooler.

At ~ 20:50 UT the brightness temperature of source #2 at 20 cm reached a peak of 2.5×10^6 K, in agreement with the X-ray results. The source then faded to $T_b \approx 1 \times 10^6$ K in about 25 minutes. This decay paralleled the decreasing ratio of the higher to lower energy MONEX (or GOES) channels. SOLEX was in the large raster mode during this time, so changes in the soft X-ray line emission cannot be assessed. It is interesting to note, however, that the Fe XVII raster at 21:28 UT (the time of minimum 20 cm flux) showed intensities almost twice those obtained at 19:55 UT, when the 20 cm flux in source #2 was higher.

4. NONTHERMAL PLASMA

As an alternative to thermal emission at 20 cm in this event, VK suggested gyrosynchrotron emission from mildly relativistic electrons trapped in magnetic loops above the active region. This possibility seems attractive for several phases of the event when source brightness temperatures differed from the electron temperatures deduced from the SOLEX, MONEX, and GOES X rays.

4.1 LIMB SOURCE

In the preceding section we have noted the decline of microwave source #2 to a minimum value of $T_b \approx 1 \times 10^6$ K at approximately 21:25 UT. Following this, the source brightness temperature increased to $T_b \approx 4 \times 10^6$ K by 21:55 (Figure 1). The flux increased by about the same factor. During this microwave rise the counting rates in all MONEX channels fell, and the spectrum softened. The cooler component observed in X rays by SOLEX did not change appreciably before 21:45, by which time the 20 cm flux had doubled from its minimum value. This can be seen from Figure 3 and Table II -- the O VII and Mg XI rasters recorded at ~ 21:33 were virtually identical to those at ~ 21:45. It appears, therefore, that much of the flux from source #2 was of nonthermal origin, probably at relatively low harmonics of the gyrofrequency. Pre-existing magnetic loops may have become populated with mildly relativistic electrons during the 30-minute flux increase. This suggestion is consistent with the lack of gross change in the region's X-ray morphology, but it must be remembered that the spatial resolution, especially of SOLEX B, is rather coarse.

4.2 DISK SOURCES

Another likely candidate for nonthermal emission is source #1 at about
20:55 and 21:25 when it had T_b(max) $\approx$ 4 x 10^6 K and 5.5 x 10^6 K, respectively
(see Fig. 1). The first event may be associated (temporally) with the M1
flare, but as we have seen, the X-ray images (during the declining phase) show
a different location (the limb) than the source #1 position (near the fila-
ment). Since P78-1 was in darkness at 20:55, we are unable to say more about
this peak of source #1. However, the second peak of source #1 occurred during
the large rasters, and as Figure 2d shows, the X-ray emission was relatively
weak at the location of source #1. The emission measures in that region were
about an order of magnitude weaker in O VII and Mg XI than those of the limb
source. We note that the MONEX LEM data show a sudden increase at 21:17 UT
and a sudden decrease at 21:25. We attribute this to a data artifact and not
to any event on the sun.

There were also two peaks in 20 cm flux in source #3 (at ~ 20:55 and
21:55), located to the northeast of the other sources. The large rasters show
no detectable X-ray flux at this site, but the location was outside the field
of the small rasters so we cannot be sure about X-ray sources at the times of
the peaks. Nonetheless, the rise and fall of source #3 (see Fig. 1) is simi-
lar to the rise and fall of source #2, which as we have argued above, is of
nonthermal nature. It therefore seems probable that the two sources were
connected by magnetic field lines. In fact the photospheric magnetogram
(Solar Geophysical Data, 1979b) suggests that a magnetic connection was pos-
sible from the leader polarity of McMath 16014 (on the disk) to the trailer
polarity of McMath 15999 (near the limb). In this scenario, source #1 is a
loop system (see VK) rooted beneath the source 2-3 loop.

5. DISCUSSION AND CONCLUSIONS

In comparing spatially resolved microwave and soft X-ray emission associated with a flare loop event, we have identified both thermal and nonthermal sources. At 20:50 UT, the time of maximum 20 cm flux from the source (#2) associated spatially with the declining X-ray flare, as much as one-half of the 20 cm flux may have been thermal bremsstrahlung from the X-ray "post-flare" loops. The rest of the emission in the 20 cm maps at that time was not associated spatially with X-ray features, and was probably of nonthermal origin. Subsequent increases in the flux from source #2 (at least) were apparently unrelated to the soft X-ray source with temperature $\sim 3 \times 10^6$ K, since the X-ray emission did not change in connection with the radio emission. The explanation that the 20 cm peaks arose from material that was so hot ($\gtrsim 1.3 \times 10^7$ K) that it produced no signature in the SOLEX rasters is implausible, for there were no observed increases in the MONEX LEM flux. Thus, we conclude that after the decline of the thermal source (by 21:25 UT) almost all of the emission must have been of nonthermal origin, probably as part of a separate event involving mildly relativistic electrons in large-scale magnetic structures connecting the two active regions in the field of view. This is consistent with the interpretation (given by VK) of the 20 cm burst as being a type IV source.

REFERENCES

Bregman, J. D., and Felli, M.: 1976, Astron. Astrophys. 46, 41.

Drago, F., and Palagi, F.: 1980, Radio Physics of the Sun (eds. Kundu and Gergely), I.A.U. Symposium No. 86 (Dordrecht: D. Reidel).

Guidice, D. A. and Castelli, J. P.: 1975, Solar Phys. 44, 155.

Kahler, S. W.: 1979, Solar Phys. 62, 347.

Kane, S. R., and Pick, M.: 1976, Solar Phys. 47, 293.

Kundu, M. R.: 1965, Solar Radio Astronomy (New York: Interscience).

Landecker, P. B., Chater, W. T., Howey, C. K., McKenzie, D. L., Rugge, H. R., Williams, R. L., and Young, R. M.: 1979, Aerospace Corporation Report TR-0080(5960-01)-1.

Landecker, P. B., and McKenzie, D. L.: 1980, Astrophys. J. (Letters) 241, L175.

Landecker, P. B., McKenzie, D. L., and Rugge, H. R.: 1979, Proc. Soc. Photo-Opt. Instrum. Eng. 184, 285.

Landini, M., and Monsignori Fossi, B. C.: 1979, Astron. Astrophys. 72, 171.

McGrath, J. F. Jr.: 1968, Rev. Sci. Instrum. 39, 1036.

McKenzie, D. L., and Landecker, P. B.: 1981, Astrophys. J. 248, 1117.

McKenzie, D. L., and Landecker, P. B.: 1982, Astrophys. J. 254, 309.

Sheeley, N. R., Jr., et al. (12 co-authors): 1975, Solar Phys. 45, 377.

Solar Geophysical Data: 1979a, 423, Pt. II (Boulder: U.S. Dept. of Commerce).

Solar Geophysical Data: 1979b, 419, Pt. I (Boulder: U.S. Dept. of Commerce).

Velusamy, T., and Kundu, M. R. (VK in the text): 1981, Astrophys. J. 243, L103.

LABORATORY OPERATIONS

The Laboratory Operations of The Aerospace Corporation is conducting exper-
imental and theoretical investigations necessary for the evaluation and applica-
tion of scientific advances to new military space systems. Versatility and
flexibility have been developed to a high degree by the laboratory personnel in
dealing with the many problems encountered in the nation's rapidly developing
space systems. Expertise in the latest scientific developments is vital to the
accomplishment of tasks related to these problems. The laboratories that con-
tribute to this research are:

Aerophysics Laboratory: Launch vehicle and reentry aerodynamics and heat
transfer, propulsion chemistry and fluid mechanics, structural mechanics, flight
dynamics; high-temperature thermomechanics, gas kinetics and radiation; research
in environmental chemistry and contamination; cw and pulsed chemical laser
development including chemical kinetics, spectroscopy, optical resonators and
beam pointing, atmospheric propagation, laser effects and countermeasures.

Chemistry and Physics Laboratory: Atmospheric chemical reactions, atmo-
spheric optics, light scattering, state-specific chemical reactions and radia-
tion transport in rocket plumes, applied laser spectroscopy, laser chemistry,
battery electrochemistry, space vacuum and radiation effects on materials, lu-
brication and surface phenomena, thermionic emission, photosensitive materials
and detectors, atomic frequency standards, and bioenvironmental research and
monitoring.

Electronics Research Laboratory: Microelectronics, GaAs low-noise and
power devices, semiconductor lasers, electromagnetic and optical propagation
phenomena, quantum electronics, laser communications, lidar, and electro-optics;
communication sciences, applied electronics, semiconductor crystal and device
physics, radiometric imaging; millimeter-wave and microwave technology.

Information Sciences Research Office: Program verification, program trans-
lation, performance-sensitive system design, distributed architectures for
spaceborne computers, fault-tolerant computer systems, artificial intelligence,
and microelectronics applications.

Materials Sciences Laboratory: Development of new materials: metal matrix
composites, polymers, and new forms of carbon; component failure analysis and
reliability; fracture mechanics and stress corrosion; evaluation of materials in
space environment; materials performance in space transportation systems; anal-
ysis of systems vulnerability and survivability in enemy-induced environments.

Space Sciences Laboratory: Atmospheric and ionospheric physics, radiation
from the atmosphere, density and composition of the upper atmosphere, aurorae
and airglow; magnetospheric physics, cosmic rays, generation and propagation of
plasma waves in the magnetosphere; solar physics, infrared astronomy; the
effects of nuclear explosions, magnetic storms, and solar activity on the
earth's atmosphere, ionosphere, and magnetosphere; the effects of optical,
electromagnetic, and particulate radiations in space on space systems.

• • •